An *ab initio* Description of the Excitonic Properties of LH2 and their Temperature Dependence

Lorenzo Cupellini,[*,†] Sandro Jurinovich,[*,†] Marco Campetella,[†] Stefano Caprasecca,[†] Ciro A. Guido,[†] Sharon M. Kelly,[‡] Alastair T. Gardiner,[¶] Richard Cogdell,[¶] and Benedetta Mennucci[*,†]

Dipartimento di Chimica e Chimica Industriale, University of Pisa, Via G. Moruzzi 13, I-56124 Pisa, Italy, Life Sciences Biomolecular Sci, Joseph Black Building, Glasgow G12 8QQ, and Glasgow Biomedical Research Centre, Institute of Molecular Cell and Systems Biology, University of Glasgow, 126 University Place, Glasgow, G12 8TA

E-mail: lorenzo.cupellini@for.unipi.it; sandro.jurinovich@for.unipi.it; benedetta.mennucci@unipi.it

[*]To whom correspondence should be addressed

[†]Dipartimento di Chimica e Chimica Industriale, University of Pisa, Via G. Moruzzi 13, I-56124 Pisa, Italy

[‡]Life Sciences Biomolecular Sci, Joseph Black Building, Glasgow G12 8QQ

[¶]Glasgow Biomedical Research Centre, Institute of Molecular Cell and Systems Biology, University of Glasgow, 126 University Place, Glasgow, G12 8TA

Abstract

The spectroscopic properties of light-harvesting (LH) antennae in photosyntehtic organisms represent a fingerprint that is unique for each specific pigment-protein complex. Because of that, spectroscopic observations are generally combined with structural data from X-ray crystallography to obtain an indirect representation of the excitonic properties of the system. Here, an alternative strategy is presented which goes beyond this empirical approach and introduces an ab initio computational description of both structural and electronic properties and their dependence on the temperature. The strategy is applied to the peripheral light-harvesting antenna complex (LH2) present in purple bacteria. By comparing this model with the one based on the crystal structure, a detailed, molecular level, explanation of the absorption and circular dichroism (CD) spectra and their temperature-dependence is achieved. The agreement obtained with the experiments at both low and room temperature lays the groundwork for an atomistic understanding of the excitation dynamics in the LH2 system.

1 Introduction

In most photosynthetic organisms light-harvesting (LH) antennae are made of pigment-protein complexes, where light is absorbed by an ensemble of interacting dyes (the pigments) arranged in a well defined three-dimensional structure determined by the embedding protein matrix. Many different types of LH complexes exist in nature, each with its own composition in terms of type and number of interacting pigments. The relative orientation and inter-pigment distances, as well as the individual interactions of the pigments with the protein matrix, are also very variable. As a result, the spectroscopic properties become a fingerprint that is unique for each specific LH complex. The absorption and circular dichroism (CD) spectra can be used, therefore, to obtain fundamental information about the structure of the complex and the electronic interactions among all the components (the pigments, the protein matrix and the external environment).

Over the last few decades, the structures of many natural LH antennae have been determined by X-ray crystallography. This has opened the possibility of obtaining an atomistic-level description of the system. By combining these structural data with spectroscopic observations it has been possible to obtain an indirect representation of the electronic properties of the system.[1–4] However, this strategy has some limitations: first of all, the crystal structure is not fully representative of the *in vivo* conditions, where temperature-dependent structural fluctuations, especially, play a fundamental role. Moreover, a large and accurate set of spectroscopic data has to be available to obtain a faithful picture.

Here, an alternative strategy is proposed, whereby molecular dynamics (MD) simulations of the pigment-protein complex within its natural environment is combined with quantum-mechanical (QM) descriptions of the electronic properties. The potentialities of such a computational approach are evident: not only can it reproduce the spectra *ab initio*, i.e. without the need of any experimental parameter, but it can also give access to the fundamental relationship between the structure, the composition of the system and its biological function.

Clearly, for such an approach to be reliable, both its components, namely the MD simulation and the QM description, should be accurate. Unfortunately, the complexity and the large dimensions of the system prevent the application of state-of-the-art QM methodological tools, and approximate models need to be used. First of all, a realistic sampling of the configurational space compels to carry out simulations based on purely classical Molecular Mechanics (MM). Moreover, the full set of interacting pigments is too large to allow for a full QM description, and an excitonic approach needs to be introduced, where the electronic properties of the full system are reconstructed from those of the single pigments and their interactions.[5]

In the Pisa group we have developed a QM excitonic approach where the effects due to the protein and the external environment are also

introduced in terms of a polarizable medium: each atom of the protein/environment is described by a point charge and an atomic polarizability; the latter generates an induced dipole in response to an applied electric field.[6] As a result of this approach, from now on called QM/MMPol, mutual polarization effects between the classical and the QM subsystem can be accounted for, and a more complete description of the environment is obtained. The protocol combining MD and the QM/MMPol excitonic approach is here used to obtain an *ab initio* simulation of the excitonic states of the peripheral light-harvesting antenna complex (LH2) present in purple bacteria, and of the resulting temperature-dependent absorption and circular dichroism (CD) spectra.

The LH2 systems of purple bacteria have been extensively studied with *ab initio* theoretical approaches, using various QM methods and making use of different techniques to compute the interactions (electronic couplings) between pigments' excitations,[7–12] as well as different models for the inclusion of the protein effects. Some of these works investigated the effect of specific protein residues, such as the Mg-binding His and the H-bonding ligands;[8,11] others described the protein environment as a dielectric medium,[9] or with point charges.[12,13] Nevertheless, a comprehensive description of the role of the protein and its temperature-dependence has not been achieved yet. In particular, what has been neglected so far is the response of the embedding system (the protein but also the surrounding lipid membrane) to the pigments' excitations. Such a response is instead very important as it can differently couple to the excitation of the individual pigments and also largely change their interactions in a non homogeneous way.[14–16] Our QM/MMPol excitonic strategy can not only account for such mutual polarization effects between the QM pigments and the environment but, by maintaining an all-atom description of the latter, can properly describe all the heterogeneities and the possible specific interactions between the pigments and the protein residues. Moreover, only a polarizable model is able to capture the explicit effect on the electronic couplings due to the environment, which can screen (or enhance) the total interaction.

The combination of this detailed description of the embedding system with a Density Functional Theory (DFT) representation of the electronic properties of the pigments allows a direct comparison to experimentally derived quantities, such as the excitonic splittings, and to the absorption and CD spectra, without the need of any further refinement or fitting procedure. Moreover, the *ab initio* nature of the model can be used to dissect the final spectroscopic response of the complex into the physical parameters which are known to determine it (site energies, couplings, temperature-dependent fluctuations, bulk and specific environment effects, etc.), thus allowing a molecular-level interpretation of their individual role and a quantification of any possible synergistic effect.

To achieve a more complete analysis, the simulations have been repeated in two different conditions, using first the crystal structure, and then the geometries extracted from a room-temperature sampling, carried out through an MD simulation of the LH2 complex within a solvated lipid membrane. In both cases the LH2 of *Rps. acidophila* has been considered. Environment effects on both electronic and structural parameters are included in all the steps of the simulation allowing a detailed understanding of the excitonic structure and its dependence on the thermal fluctuations of the system. The agreement obtained with the spectroscopic data at both low and room temperature shows the reliability of the calculated exciton parameters which lay the groundwork for an atomistic understanding of the excitation dynamics in the LH2 system.

2 Methods

2.1 LH2 structure

LH2 complexes are characterized by a cylindrical structure of C_n symmetry (n = 8, 9 or 10, in *Rps. acidophila* $n = 9$) where the monomer units are composed of low-molecular weight proteins, and bacteriochlorophyll *a* (BChl) and

carotenoids as absorbing pigments.[17] Within the LH2, the BChls responsible for the low-energy part of the absorption spectrum are arranged in two rings. One ring contains nine BChls, whose molecular plane is perpendicular to the C_9 axis, and is responsible for the peak at 800 nm. The second ring, which is instead responsible for the 850 nm peak, contains 18 BChls, whose molecular plane is perpendicular to the cylinder radius (see Figure 1).

The crystal structure of the LH2 complex from *Rps. acidophila* (PDB code: 1NKZ) resolved at 2.0 Å was used[18] (see Figure 1a). This structure has a 3-fold symmetry, *i.e.*, only the atomic coordinates of one third of the entire ring are explicitly contained in the PDB file. This third contains three repeating units which are not perfectly identical, so that this crystal structure does not have perfect C_9 symmetry. The complete ring of LH2 has been reconstructed using the transformation matrix contained in the PDB file. Hydrogen atoms were added by using the *LeAP* module of AmberTools considering all the titrable residues in their standard protonation state. All Histidine residues were kept in the ϵ configuration except those axially coordinated with the B850 BChls. The positions of the hydrogen atoms were optimized at MM level using Amber14.[19]

A mixed QM/MM relaxation was carried out, where three selected BChls (302-β, 303-α & 307-γ) were treated at QM level, and the remaining atoms were kept frozen at their position in the crystal structure.

2.2 Molecular Dynamics

We applied the same procedure devised by Ogata et al.[20] for the simulation of the entire Photosystem II embedded in a phospholipid membrane. For each moiety of the system we used specific force field parameters. The lipid14[21] force field has been used for the lipids, and the ff99SB[22] for the protein. The parameters for the BChls were taken from the literature,[23] while an approach recently developed in our group using a DFT-based strategy[24] was used for the carotenoids. Water molecules were described by the TIP3P model. In the first step the starting structure was built by embedding the LH2 system in a lipid bilayer composed by 2-oleoyl-1-palmitoyl-sn-glycero-3-phosphocholine (POPC), and subsequently surrounding the membrane with two layers of water (TIP3P). The VMD suite of tools was used.[25] Starting from this structure, a classical molecular dynamics (MD) was performed, following the protocol shown below, and using the Amber14 suite of programs.[19]

The whole system ($\sim$ 225 000 atoms) was first minimized, and then thermalized in two steps, by running a 5 ps NVT simulation from 0 to 100 K, and then a 100 ps NPT simulation up to 300 K, constraining the protein, cofactors, and lipids with a harmonic potential (10.0 kcal mol^{-1} Å^{-1}). The 10 ns NPT equilibration was performed, gradually releasing the harmonic constraints, until a constant density was reached. Finally, the simulation was extended for a 100 ns production. For all simulations, the timestep was set to 2 fs. The temperature and pressure were controlled, respectively, by a Langevin thermostat and the anisotropic barostat implemented in Amber14. The RMSD of the protein backbone and BChl rings of the production run is reported in Figure S1 of the Supporting Information. After the first 20 ns, we considered the system equilibrated. Further details about the MD simulation are reported in the Supporting Information.

2.3 Quantum Mechanical calculations

All QM calculations have been performed using a locally modified version of the Gaussian G09 suite of programs.[26] Electronic couplings were computed using a well-established method based on the transition densities of the interacting moieties.[6,27,28] The symmetry of the system allows the calculations to be simplified by taking into account the equivalence of BChls within the LH2 symmetric structure (see Figure 1b): the couplings between equivalent pairs have been equalized to their average value.

In all excited state calculations, we employed time-dependent density functional theory (TD-DFT) with the CAM-B3LYP functional and

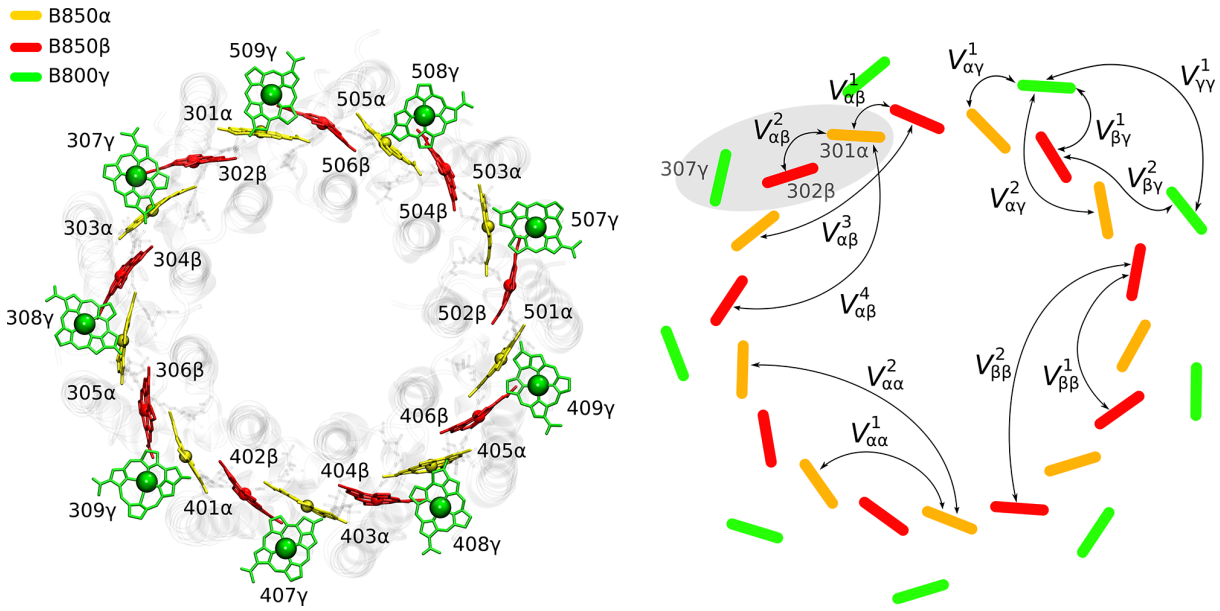

Figure 1: Left: Molecular structure of LH2. BChls are highlighted using the following color code: yellow for B850α, red for B850β, green for B800γ. Right: Electronic coupling map. The superscript ranks proximity according to center-center BChl distance. Note that the system has a C9 symmetry and the labels for equivalent coupling terms are reported only once. The repeating unit is highlighted in gray and the corresponding BChl labels have been also reported for clarity. Coupling less than 10 cm^{-1} are not indicated as not included in the exciton Hamiltonian.

the 6-31G(d) basis set. This functional is best suited for the description of charge-transfer states, while also providing accurate excitation energies and dipole strengths for the Q_y states of BChls, in good agreement with multireference benchmarks.[29]

To describe the effects of the environment we employed a polarizable QM/MM model (QM/MMPol). Here, the environment consists in all the BChl units not in the QM calculation, the carotenoids, the protein, and, for the analysis on the MD trajectory, the lipid membrane, the water molecules, and the counterions. In the QM/MMPol model, the environment is described classically in terms of fixed atomic charges and induced dipoles.[28] The latter, in particular, make the whole QM/classical scheme fully polarizable, which implies that not only the QM density is perturbed by the environment, but the environment itself is able to respond to its presence. A cutoff of 12 Å from the heavy atoms of the QM BChl ring was used to define the polarizable MM region, whereas all the other atoms in the simulation box were considered non-polarizable. The current implementation of the MMPol model within Gaussian includes the electrostatic and polarization effects of the environment on both the ground and excited states, as well as on the electronic couplings. Additional *in vacuo* calculations (VAC) have been performed, where only the BChl of interest is considered without any environment.

The excitonic Hamiltonian describing the multichromophoric system was built from the BChl site energies ϵ and their electronic couplings V:

$$\hat{H} = \sum_n \epsilon_n |n\rangle \langle n| + \sum_{mn} V_{mn} |n\rangle \langle m| \qquad (1)$$

where both elements contain the effect of the environment. All the excitonic analyses were performed by using EXAT,[30] a program developed in our laboratory. Due to the small basis set used for the single-chromophore TD-DFT calculations (vide supra), the rotatory strength of the excitonic states were computed using the approximate version of the excitonic Rosenfeld

equation:

$$R_{0K} = -\frac{\pi\tilde{\nu}_k}{c}\sum_{i>j}^{N} C_i^K C_j^K \mathbf{R}_{ij}\cdot(\boldsymbol{\mu}_i \times \boldsymbol{\mu}_j) \quad (2)$$

where index K identifies the excitonic state, whereas indexes i and j run over the N chromophores. Vectors $\boldsymbol{C}^K$ are the excitonic coefficients of state K in the expansion over the BChl basis, $\mathbf{R}$ is the vector-distance between two BChl units, and $\boldsymbol{\mu}$ their transition dipoles. The midpoint between the NB–ND atoms of each BChl is considered as the center of the chromophore when the distances $\mathbf{R}_{ij}$ are computed. For further details about the excitonic approach to the rotatory strength in EXAT, we refer to Ref.[31]. Here we only point out that test calculations using a complete magnetic-electric approach with an extended basis set essentially give the same results. These data are shown in Figure S6 of the Supporting Information.

To account for possible charge-transfer effects between strongly coupled BChls, we resorted to the fragment charge difference (FCD) scheme, in its multistate formulation (MFCD),[32] applied to BChl dimers in the B850 ring. In the MFCD, the diabatic states are defined as those that either maximize or minimize the charge difference between donor and acceptor fragments. The transformation from the adiabatic to the diabatic basis can be obtained by diagonalizing the Δq matrix, whose elements are defined as:

$$\Delta q_{mn} = \int_{r\in\mathrm{D}} \rho_{mn}(r)\ \mathrm{d}^3r - \int_{r\in\mathrm{A}} \rho_{mn}(r)\ \mathrm{d}^3r \quad (3)$$

where $\rho_{mn}(r)$ is the transition density between states m and n, with $n \neq m$, or the state density if $m = n$. This procedure returns diabatic-like states and their couplings.

2.4 Modeling of linear spectra

In order to reproduce the spectral broadening, in the computation of linear absorption (LA) and circular dichroism (CD) spectra, lorentzian lineshapes were used. The half-width at half-maximum (HWHM) was taken as the experimental value measured at 77K, namely 120 and 85 cm^{-1} for the B850 and B800 bands, respectively. In the MD simulation, a different Hamiltonian matrix was obtained for each snapshot, and we modeled the instantaneous spectra as previously described. The total spectrum was then obtained by averaging the spectra corresponding to each snapshot. We approximated the inhomogeneous broadening in terms of the "pure" contribution of the environment. This can be defined as the standard deviation of the solvatochromic shift:

$$\sigma_{\mathrm{env}}^2 = \langle(E_{\mathrm{MMPol}} - E_{\mathrm{VAC}})^2\rangle - \langle(E_{\mathrm{MMPol}} - E_{\mathrm{VAC}})\rangle^2 \quad (4)$$

where E_{MMPol} and E_{VAC} are the energies obtained with the environment and *in vacuo*, respectively. The MMPol site energies were then corrected to obtain a new distribution with a reduced standard deviation σ_{env}. Namely, the new site energies E_i' are obtained by reducing their distance from the average site energy $\langle E\rangle$:

$$E_i' = (E_{i,\mathrm{MMPol}} - \langle E\rangle)\frac{\sigma_{\mathrm{env}}}{\sigma} + \langle E\rangle \quad (5)$$

where σ is the standard deviation of the original site energy distribution. We note that such an inhomogeneous broadening also contains homogeneous components as these two cannot be decoupled in our approach where the fluctuations of site energies are those determined by the MD trajectory. This estimate of the inhomogeneous broadening is therefore an upper limit of the real value. The homogeneous broadening was arbitrarily fixed to lorentzian lineshapes with the same widths of the fitted low temperature absorption spectrum. We assigned an HWHM of 120 cm^{-1} for the exciton states mainly delocalized on B850 pigments and 85 cm^{-1} for those delocalized on the B800 pigments (the assignment of the exciton states was carried out on the basis of $|C^K|^2$ composition). To estimate the sensitivity of the spectrum to this parameter, we compared the average spectra computed with different values of the homogeneous linewidths (See Figure S11 in the Supporting Information).

3 Results

The results are organized into two sections, one referring to the crystal structure and the other to the MD simulation. All the results are finally put together and commented in the Discussion.

3.1 Crystal structure

3.1.1 Excitonic approximation and the role of charge transfer states

The validity of the excitonic model for the LH2 was tested by comparing the excitonic properties (Exc) of three $\alpha\beta$ dimers, composed of BChls with indexes 506, 301, 302, and 303 (see Figure 1), with the corresponding full-QM (fQM) calculations. This analysis was carried out both *in vacuo* (VAC) and in the presence of the polarizable environment (MMPol). In the case of fQM calculations, VAC model naturally includes the mutual polarization between the two BChls which is instead neglected in the excitonic VAC model. The resulting exciton splittings between the two lowest bright Q_y states are reported in Table 1.

Table 1: Excitonic (Exc) and full-QM (fQM) splittings (cm^{-1}) *in vacuo* (VAC) and including the environment (MMPol) for 3 selected dimers. Exc-CT refers to a super-excitonic scheme, where the coupling between the excitonic Q_y states and the CT states is also considered

	VAC		MMPol		
Dimers	Exc	fQM	Exc	Exc-CT	fQM
301–302	693	853	753	843	863
301–506	585	765	819	921	908
302–303	734	903	911	1016	1009

The agreement is quite good for all the three dimers, with the excitonic model generally slightly underestimating the full QM results. Although dimers 301–506 and 302–303 are of the same type, they are slightly different, because of the non-perfect symmetry of the crystal structure. We note that the presence of all the other BChl units, introduced through the MMPol together with the rest of the environment (protein and other cofactors), changes the transition density and provides results closer to the full QM ones. Indeed, the ability to reproduce the full QM splittings consistently increases from 80 to 90% moving from *in vacuo* to MMPol data.

The missing 10% might be induced by charge-transfer (CT) states, which are not explicitly taken into account in the excitonic model. To verify this hypothesis, we have performed the following analysis. Starting from the full QM calculations on each dimer, we applied the MFCD approach described in the previous section to compute the couplings between four electronic excited states: the first two Q_y and the first two CT states (see the Computational details). From this analysis, we calculated that the CT states lie above the Q_y states in all dimers; however, the couplings between the lowest Q_y and the CT states are nearly half of the energy difference (see Table S1 in the Supporting Information). Therefore we can expect a stabilization of the lowest Q_y due to the CT states, which would not be accounted for in the monomer-based excitonic model. In order to quantify this effect, we adopt a super-excitonic scheme, where the coupling between the excitonic Q_y states and the CT states are also considered. The following matrix is diagonalized:

$$H = \begin{pmatrix} E(Q_{y1}) & 0 & V_{11} & V_{12} \\ 0 & E(Q_{y2}) & V_{21} & V_{22} \\ V_{11} & V_{21} & E(CT_1) & 0 \\ V_{12} & V_{22} & 0 & E(CT_2) \end{pmatrix} \quad (6)$$

where $E(Q_{y1,2})$ are the excitonic energies of the dimer, while $E(CT_{1,2})$ and V are the energies of the CT states and their couplings with the Q_y respectively, as obtained with the MFCD scheme (the values of the matrix elements used in the Exc* calculations are reported in Table S2 of the Supporting Information). The diagonalization of the matrix results in a new set of four states. The splittings between the new excitonic states are reported in the last column of Table 1 (Exc-CT). They are much closer to the full QM ones, indicating that indeed the

small discrepancy previously observed was due to charge transfer states.

In addition to affecting the excitonic energies, the presence of CT states could also modulate the excitonic properties of the aggregate. We therefore estimated the contribution of the CT states to the wavefunction of the dimers. Starting from a full QM description, this estimate was performed by analyzing the MFCD coefficients, *i.e.*, the contribution of the localized and CT states on the adiabatic states. The results are summarized in Table 2. The lowest state is the one most affected by the CT mixing (∼3%). The two CT states contribute with approximately the same weight. Very similar results are obtained extending the model to the tetramer formed by two dimers: this shows that the results converge with respect to the size of the cluster considered and to the relative number of CT states included (2 for the dimer, 6 in the case of the tetramer). The small contribution found in all cases indicates that the CT mixing does not significantly affect the properties of the Q_y excitonic states, and therefore, in the following sections, it will no longer be considered in the simulation of the properties of the full LH2 aggregate.

Table 2: Multistate FCD (MFCD) coefficients of various diabatic transitions in the first Q_y adiabatic state of two BChl dimers (D) (crystal structure, environment included at MMPol level). The corresponding values in the tetramer (T) are also reported.

State	D	T	% D	% T
301-302				
Q_{y1} (302)	0.98	0.99	97	98
Q_{y2} (301)	0.01	0.00	0	0
CT_1 (301-302)	-0.14	-0.11	2	1
CT_2 (302-301)	0.12	0.11	1	1
301-506				
Q_{y1} (506)	0.99	-0.99	97	98
Q_{y2} (301)	0.01	-0.01	0	0
CT_1 (301-506)	-0.11	0.08	1	1
CT_2 (506-301)	-0.13	-0.10	2	1

3.1.2 Excitonic parameters and exciton energies

In Table 3 we report the QM/MMPol parameters of the excitonic Hamiltonian based on the crystal structure.

Table 3: Site energies and couplings (in cm^{-1}) computed on the crystal structure. See Figure 1 for the definition of the couplings. The signs of the couplings are consistent with transition dipoles pointing towards the NB → ND direction.

Site energy	B850α	11251
	B850β	10987
	B800γ	11389
Intra-B850	$V^1_{\alpha\beta}$	409
	$V^2_{\alpha\beta}$	362
	$V^3_{\alpha\beta}$	25
	$V^4_{\alpha\beta}$	24
	$V^1_{\alpha\alpha}$	-87
	$V^2_{\alpha\alpha}$	-14
	$V^1_{\beta\beta}$	-59
	$V^2_{\beta\beta}$	<10
B850-B800	$V^1_{\alpha\gamma}$	59
	$V^2_{\alpha\gamma}$	-20
	$V^1_{\beta\gamma}$	-12
	$V^2_{\beta\gamma}$	<10
Intra-B800	$V^1_{\gamma\gamma}$	-50

The calculated site energies of B850α and B850β are slightly different, the α BChl lying 265 cm^{-1} higher than the β. This energy difference is however smaller than the excitonic coupling between first neighbors (409 cm^{-1}), resulting in very little impact on the expansion coefficients of the exciton states. The coupling between second neighbors are much smaller than the first ones, but not at all negligible. When moving to the inter-ring properties, we see that the energy difference between B800–B850α and B800–B850β is always larger than their couplings. As a result a very small mixing is found for the states localized on the two rings.

Moving to the analysis of the couplings in the B850 ring, we note that the nearest-neighbor

inter-dimer couplings ($V^1_{\alpha\beta}$) are larger than the intra-dimer couplings ($V^2_{\alpha\beta}$). This result is apparently in contradiction with previous studies on both *Rps. acidophila*[7,8,11,33] and *Rps. molischianum*[9,10] complexes (see Table S5 in the Supporting Information for a complete comparison with the literature). However, the same couplings when calculated without the inclusion of the polarizable environment do reproduce what is found in the literature: in particular, our *in vacuo* nearest-neighbor couplings are close to those of Scholes *et al.*,[8] computed at the CIS/6-31G* level, but rescaled to match the experimental transition dipoles.

The inversion of $V^1_{\alpha\beta}$ and $V^2_{\alpha\beta}$ arises from the environmental screening of the Coulomb interaction, which is different for the two pairs (see below). It is worth noting that the same difference between *in vacuo* and MMPol calculations is observed also for the dimer splittings (see Table 1). The couplings between more distant pairs are slightly larger than those calculated in the previous studies on *Rps. acidophila*,[7,11] the reason for this probably being the different QM method employed here.

From these parameters the Hamiltonian matrix was built as in Eq. 1 and diagonalized, obtaining the excitonic states: the corresponding eigenenergies are shown in Table S3 of the Supporting Information together with the squared transition dipoles and rotatory strengths. Given the small inter-ring mixing, it is possible to separate the states between those localized on the B850 ring and those localized on the B800 ring, and assign them on the basis of their symmetry. By symmetry, only the states $k = 0, \pm1, \pm8$, and 9 have a non-zero transition dipole moment. The dipole moment of states k =0 and 9 is parallel to the C_9 axis, while that of the other states lie on the ring plane. Owing to the relative orientation of dipole moments of both B850 and B800, most of the dipole strength is concentrated in the $k = \pm1$ states of either ring.

Our results show an exciton bandwidth of 1652 cm^{-1} with the B850 splitting between states $k = \pm1$ and $k = \pm8$ equal to 1517 cm^{-1}. This splitting is only 5% larger than the experimental value of 1442 cm^{-1} obtained from fluorescence anisotropy excitation measurements at 4.5K.[2] Since the B800–B850 mixing is negligible, the B850 exciton splitting is only determined by the $\alpha - \beta$ site energy difference and electronic couplings. If we use the same site energy for the α and β BChls, a small (18 cm^{-1}) decrease of the B850 splitting is observed: this means that the splitting is mainly determined by the electronic couplings.

The B800–B850 energy gap was reported to be 936 cm^{-1} at very low temperature.[3] Our B800–B850 gap is 1065 cm^{-1}. As the position of the B800 band is only slightly affected by the electronic couplings, the gap depends on the inter-B850 couplings and the B800–B850 site energy difference. Our slight overestimation of this gap is probably due to an overestimation of the inter-B850 couplings, as this could also explain the 5% larger B850 splitting.

Finally, it is worth noting that the upper B850 excitons are much closer in energy than the lower ones, resulting in an asymmetrical exciton structure, where the density of states is higher at the blue edge of the exciton band (see Figures S7 and S8 in the Supporting Information). Including only the nearest-neighbor couplings results in a symmetric exciton structure, therefore the asymmetry of the exciton band seen here is necessarily due to the second neighbor couplings.

3.1.3 Absorption and circular dichroism spectra.

Using the parameters described in the previous section, we calculated the excitonic linear absorption (LA) and circular dichroism (CD) spectra of LH2 in the near-infrared region. The LA and CD spectra are reported in Figure 2, along with the experimental data at low temperature.[1]

The LA spectrum well agrees with the experiments at 77K, except for the overestimation of the B800–B850 splitting we have discussed above. Switching off the interactions between the two rings, the excitonic energies do not change significantly, and as a result the linear absorption spectrum is almost equal to the sum of B800 and B850 contribution (see Fig-

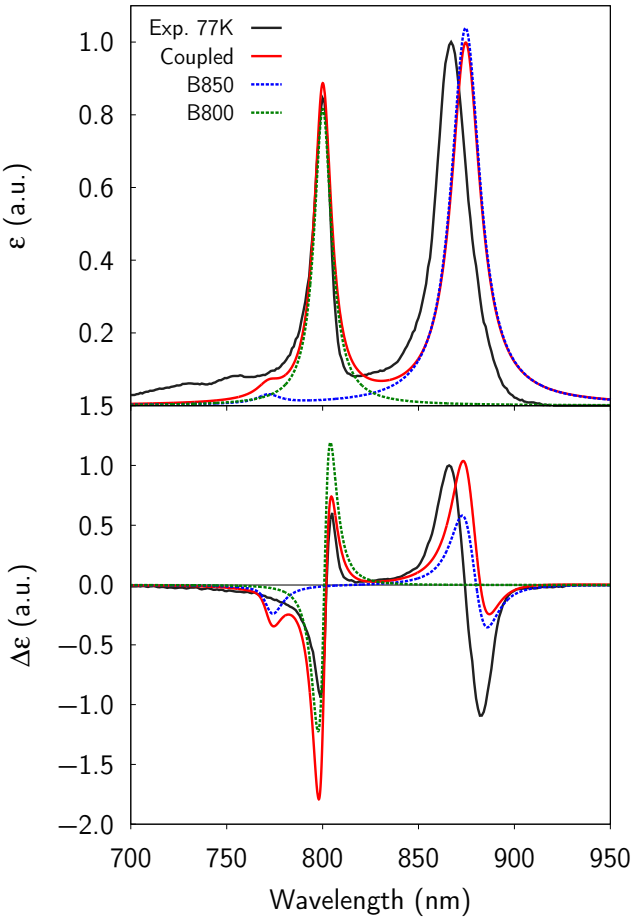

Figure 2: Excitonic LA (top) and CD (bottom) spectra of LH2 derived on the crystal structure. The absorbance and CD intensity are given in arbitrary units and normalized to the most intense positive peak. The dashed lines represent the spectra obtained for the B800 (green) and B850 (blue) rings independently. The whole spectrum was shifted in energy to match the peak at $\sim$ 800 nm (energy shift = 0.147 eV).

ure 2 top). However a small degree of mixing is responsible for a dipole strength redistribution in the coupled system resulting in a slightly different relative intensities of the B850 and B800 peaks with respect to the decoupled description.

The main features of the experimental CD spectrum, i.e. the sign of the bands and the couplet positions, are correctly reproduced by the calculations. However, in the experimental spectrum, the two couplets have a nearly symmetrical shape, whereas this is no longer true in the modeled spectrum. Unlike the LA, the CD spectrum modeled on the whole system is significantly different from the sum of the B800 and B850 components. Part of the positive rotatory strength is redistributed from the B800 to the B850 couplet due to the B800–B850 mixing. The couplings that induce this mixing ($V_{\alpha\gamma}$ and $V_{\beta\gamma}$) are relatively small, nonetheless their effect is significant in the CD spectrum. As our model is based on a non-disordered homogeneous picture, whereas static and dynamic disorders play an important role in localizing the exciton states, the B800–B850 mixing predicted by our Hamiltonian is probably overestimated. It is worth noting that the signature of this mixing is only visible in the CD spectrum, which is particularly sensitive to small changes in the composition of the excitons.

Given the particular arrangement of the pigments, the CD spectrum also shows a great sensitivity to small changes in the relative orientations of the electric transition dipole moments.[1] Because of the asymmetry of the chlorine ring in BChl, the transition dipole moment of the Q_y transition is not exactly parallel to the NB–ND direction. To quantify that, for each pigment we define an internal reference frame (see Figure 3, top) and we calculate the polar angles θ and ϕ, which indicate the angle of the dipole with the BChl plane and the NB–ND bond, respectively. The calculated transition dipoles show different θ and ϕ angles depending on the pigment class. The ϕ angle is -3.6,-2.0, and -3.6 degrees, respectively, for B850α, β, and B800, while θ is 0.1,-2.6, and -1.5 degrees. We note that the transition dipoles computed by Anda et al.[34] using a multi-reference approach (RASSCF) are much closer to the NB–ND axis; we stress however that those calculations did not include the effects of the surrounding protein.

To achieve a more detailed picture of the sensitivity of the CD on the dipole orientation, in Figure 3 we have simulated many different spectra obtained by varying the θ and ϕ angles of the different pigments. The results show that a variation of a few degrees in the orientation of the B850 dipoles can significantly change the CD spectrum and even leads to an inversion of the sign of the couplet.

Until now we have used the crystal structure

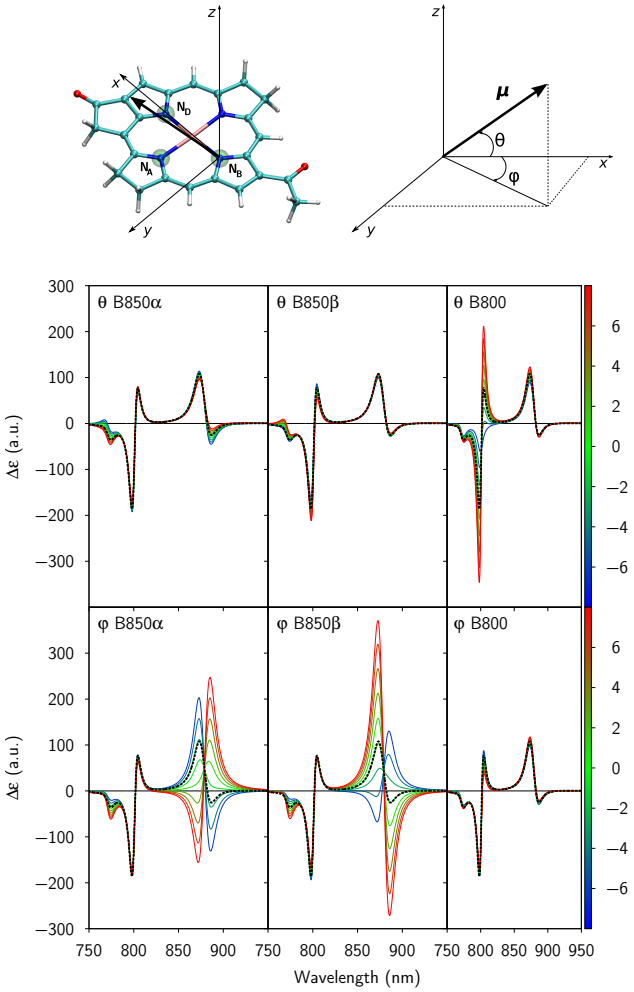

Figure 3: Top: Definition of the reference frame and of the polar angles (θ,ϕ). Bottom: CD spectra obtained for different values of θ and ϕ. Dotted black lines correspond to the original CD spectrum (without any modification).

of LH2 which corresponds to a static picture of the system, frozen in a specific conformation. We can thus expect that this model is not representative of the LH2 at room temperature. An overall LH2 structural relaxation taking into account the thermal effects can be obtained through an MD simulation. Moreover, the MD simulation also includes the bilayer lipid membrane and the solvation water molecules, and allows for a sampling of the coupled pigment-environment fluctuations at room temperature. The results of this simulation are reported in the next section.

3.2 Molecular Dynamics

The main structural parameters of the B800 and B850 rings have been monitored along the MD. To gain an insight on their size and shape, the two rings have been fitted independently with an ellipse at each snapshot. The fluctuations of the ellipses centres are plotted in Figure S2 of the Supporting Information. The values are centred around the origin and show negligible variations along the trajectory. The distribution of the B800 ring centre is more spread than that of the B850 ring, due to the fact that the latter BChls are more strongly packed within the protein. The size and shape of the rings can be analysed through the sum and difference, respectively, of the fitted semiaxes, which are plotted in Figure S4 of the Supporting Information.

The absolute value of the difference of the semiaxes, for both B800 and B850 rings, is close to zero along the dynamics, indicating that the rings remain practically circular. Elliptical distortion, fluctuating on the timescale of seconds, was invoked to explain single-molecule fluorescence experiments,[35] but obviously, our MD cannot capture the potential deformations on such long timescale. The sum of the semiaxes is also constant, indicating that the size of the rings does not vary during the dynamics. On the contrary, the B800 ring is slightly larger in the MD (∼3%) than in the crystal.

Two different 20 ns windows of the full trajectory have been selected for QM/MMPol calculations. The first window samples the production run in the range 20–40 ns, the second window samples the 80–100 ns range. A set of 44 uncorrelated snapshots was extracted from both windows, for a total of 88 snapshots. To enlarge the sampling, for all the selected frames, we averaged the site energies of the equivalent BChls and the couplings of the equivalent pairs.

3.2.1 Role of CT states

In analogy with the crystal structure case, the influence of CT states in the description of the final exciton states has been investigated by the MFCD approach (see section 2.3 for details). We considered the four lowest excited states of

the 301α–306β dimer corresponding to the two Q_y states and the two CT states. Considering the high computational cost required for the calculations, the CT analysis was limited to the first sub window of the MD simulation. The distribution of couplings and the relative CT character percentage are reported in Figure 4.

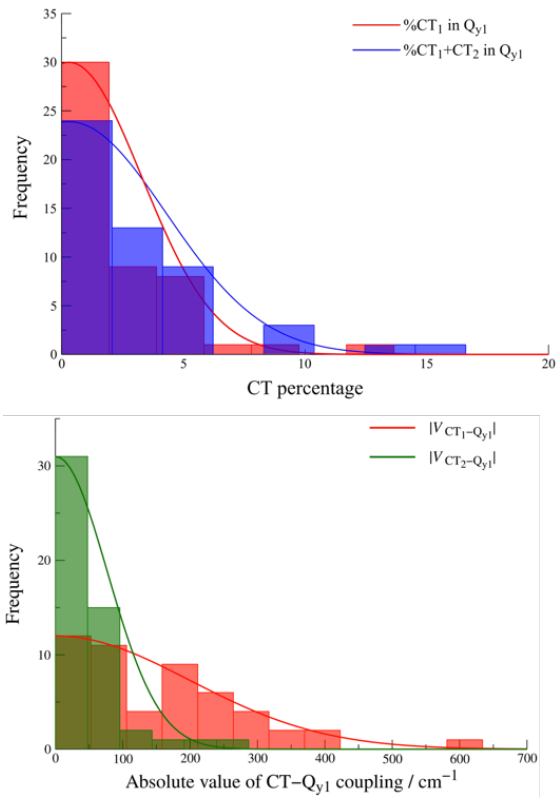

Figure 4: Upper panel: Distribution of the absolute values of MFCD couplings between the first Q_y and the first two CT excitations in a BChl dimer, computed for 50 uncorrelated frames extracted from a classical NPT MD simulation of 100 ns. Lower panel: Distribution of the CT character of the first Q_y bright transition in a BChl dimer, along 50 uncorrelated frames extracted from a classical NPT MD simulation of 100 ns.

These results show that the influence of CT in the description of the Q_y wavefunction of the aggregate is on average small and in line with what already observed in the case of the crystal structure: the CT percentage does not typically exceed 5%, and couplings are usually smaller than 400 cm^{-1}. This shows that the LH2 description by the excitonic model is accurate also in the case of structures obtained from MD simulations, at least for what concerns the absorption process.

3.2.2 Excitonic parameters and exciton energies

As done in Table 3 for the crystal structure, in Table 4, we report the excitonic parameters calculated as averages along the MD trajectory together with their standard deviations.

Table 4: Average site energies and couplings and standard deviations (σ) along the MD trajectory. For the site energies, the results obtained without including the effects of the environment are also reported (VAC). See Figure 1 for the definition of the couplings. The site energy values in parenthesis are referred to ones computed on BChls' QM/MM relaxed structure. All values are in cm^{-1}.

		E/V	σ
Site Energy (VAC)	B850α	13634	319
	B850β	13631	347
	B800γ	13633	347
Site Energy (MMPol)	B850α	12799 (13089)	393
	B850β	12806 (13051)	413
	B800γ	13021 (13350)	449
Intra-B850	$V^1_{\alpha\beta}$	317	55
	$V^2_{\alpha\beta}$	339	38
	$V^3_{\alpha\beta}$	20	2
	$V^4_{\alpha\beta}$	18	1
	$V^1_{\alpha\alpha}$	-66	6
	$V^2_{\alpha\alpha}$	-10	1
	$V^1_{\beta\beta}$	-51	6
	$V^2_{\beta\beta}$	<10	-
B850-B800	$V^1_{\alpha\gamma}$	42	4
	$V^2_{\alpha\gamma}$	-16	2
	$V^1_{\beta\gamma}$	-10	4
	$V^2_{\beta\gamma}$	<10	-
Intra-B800	$V^1_{\gamma\gamma}$	-32	4

The absolute excitation energies of the Q_y states are around 12800 cm^{-1} (780 nm),

some 1600 cm^{-1} higher than Q_y states computed for the crystal structure. To test if the origin of this energy shift is due to the enlarged environment in the MD (where also membrane lipids and water are considered together with the protein matrix) or the geometrical fluctuations, we independently relaxed three representative BChls, within the frozen crystal structure using QM/MM optimizations. The excitation energies computed on these new geometries, reported in parentheses in Table 4, are close to the average values of the MD for all the three BChls. This finding suggests that the energy shift is not related to the different environments between the crystal and the MD descriptions but it mainly depends on the internal pigment geometry. The BChl geometries along the MD trajectory fluctuate around equilibrium structures that are close to those obtained by relaxing the pigment within a frozen (i.e. crystalline) protein.

The site energy difference between B850α and B850β observed in the crystal structure vanishes when averaged along the MD trajectory. The difference becomes negligible (< 10 cm^{-1}) and the two site energy distributions show very similar values of standard deviations. This result suggests that structural and environmental fluctuations change the site energy landscape with respect to the crystal and makes the B850 average site energies almost degenerate.

Interestingly, the average site energies computed without the effect of the environment (VAC) are the same for all the BChl types (the differences are less than 5 cm^{-1}). Notably, all the BChls should present the same properties in vacuo; however, in the crystal structure, the geometries of the different BChls are slightly different, and this is reflected in the differences observed in the VAC model. These differences disappear when we average over the temperature dependent fluctuations coming from the MD trajectory. When the environmental effects are turned on in the QM/MMPol description, the site energies of B850 pigments are redshifted by about 200 cm^{-1} with respect to the B800. Therefore, the main source of site energy difference between B800 and B850 is the polarizable environment in which the pigments are embedded.

As already observed for other LH systems,[14–16] also for LH2 the calculated width of the site energy distribution is too large. The source of that can be ascribed to the MM force fields used in the MD simulation.[24] In fact, the standard deviations are mainly determined by fluctuations of the pigment geometries and not by the environmental effects: σ values remain practically unchanged when we switch off the environment effects (see VAC data) in the calculation of the site energies. To extract a more physical value of the disorder due to the environment, we computed the standard deviation of the MMPol-VAC site energy difference along the MD. The resulting σ_{env} are 120 and 146 cm^{-1}, respectively, for α and β B850 BChls, and 200 cm^{-1} for B800 BChls: the peak broadening estimated as the HWHM of a fitted lorentzian profile on the absorption spectrum at room temperature for B850 and B800 bands, is 170 cm^{-1} and 140 cm^{-1} respectively.

Passing from the crystal structure to the MD average, all couplings consistently reduce by 5 to 20% with the two largest couplings ($V^1_{\alpha\beta}$ and $V^2_{\alpha\beta}$) becoming much more similar. To explain this decrease, we recall that, in our model, the electronic coupling is composed by two terms: the Coulomb interaction between transition densities (V_{Coul}), and the MMPol screening, which depends on all the polarizable MM atoms included in the description of the system (V_{MMPol}).[5,15,28] The calculations based on the MD trajectory also include the lipid membrane and the water, which are not present in the crystal structure, possibly resulting in underestimation of the screening. To further investigate this issue, we introduce an effective dielectric constant:

$$\varepsilon_{\mathrm{eff}} = \frac{V_{\mathrm{Coul}}}{V_{\mathrm{Coul}} + V_{\mathrm{MMPol}}} \qquad (7)$$

which determines how much the coupling of each pair is screened by the polarizable environment: the more $\varepsilon_{\mathrm{eff}}$ is larger than 1, the greater is the screening. We computed the $\varepsilon_{\mathrm{eff}}$ values for all the pairs for both the CRY and MD descriptions and the results are reported in Figure 5.

As expected from the different environment

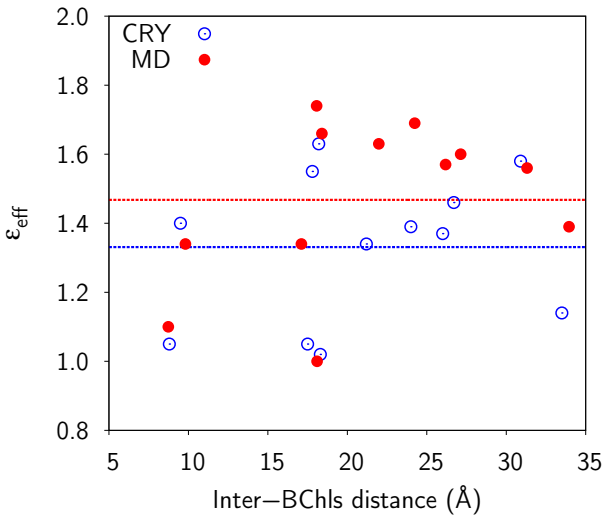

Figure 5: Effective dielectric constant for MMPol@CRY and MMPol@MD data sets. Dotted lines represents the average values of ε_{eff}.Only the pairs with a $V_{\text{Coul}} > 10$ cm^{-1} have been considered

composition in the two models, the average ε_{eff} goes from 1.33 in the crystal structure to 1.47 in the MD. However, ε_{eff} of the closest (and most strongly interacting) B850 pairs is almost equal in the two models, with the closest pair feeling an almost null screening (ε_{eff}=1.1). This analysis shows that the significant difference found in the couplings for the closest pairs ($V^1_{\alpha\beta}$ and $V^2_{\alpha\beta}$) cannot be due to the different environment included in the CRY or the MD model. Indeed, the same decrease is observed for the direct Coulomb contribution, which for $V^1_{\alpha\beta}$ reduces from 428 to 348 cm^{-1} (18%), and for $V^2_{\alpha\beta}$ reduces from 505 to 455 cm^{-1} (10%). If we adopt a point-dipole approximation (PDA), these couplings drop from 948 to 892 cm^{-1} (6%), and from 896 to 754 (16%), respectively, capturing part of the observed reduction. As the inter-pigment distance is almost unchanged for these pairs passing from the crystal structure to the MD average, the observed reduction of the coupling has to be related to a change in the distribution of the transition densities which are only partially seen by the PDA.

From the average Hamiltonian of Table 4 we computed the energies of the excitonic states (See Table S1 in the Supporting Information). The resulting splitting between the states k=±1 and ±8 of the B850 ring reduces to 1275 cm^{-1}, close to the experimental B850 splitting of 1259 cm^{-1} at 263K.[2] Notably, the trend observed moving from the crystal to the MD picture is in agreement with the experimental temperature dependence of the splitting. As we showed for the crystal, the α–β site energy difference has little effect on the B850 splitting; therefore, the difference in the excitonic splitting can only be attributed to the effect of the couplings. The experimental B800–B850 gap at room temperature is 826 cm^{-1},[3] notably smaller than the gap observed at low temperature. Our average Hamiltonian predicts a gap around 900 cm^{-1}, slightly larger than the experimental value.

3.2.3 Absorption and circular dichroism spectra

As discussed in the previous section, the MD simulation allows us to describe the disorder within the LH2 system, taking into account fluctuations of site energies, coupling and transition dipole moments. This disorder will be reflected in the excitonic states and in the corresponding properties which determine the spectra. To closely inspect the effects of the disorder, in Figure 6 we report the average spectra superimposed to all the instantaneous spectra calculated for every MD frame. While the LA is merely broadened by the disorder, the out-of-phase sum of the CD spectra greatly reduces the intensity of all the bands. The strong inter–B850 coupling prevents significant mixing of B850 excitons and the consequent spread of oscillator strength. On the contrary, for the B800 ring, the disorder has a large effect on the intensity of the CD bands, which become weaker than the B850 couplet.

Finally, the average LA and CD spectra are compared to the experimental ones measured at room temperature; the comparison is reported in Figure 7.

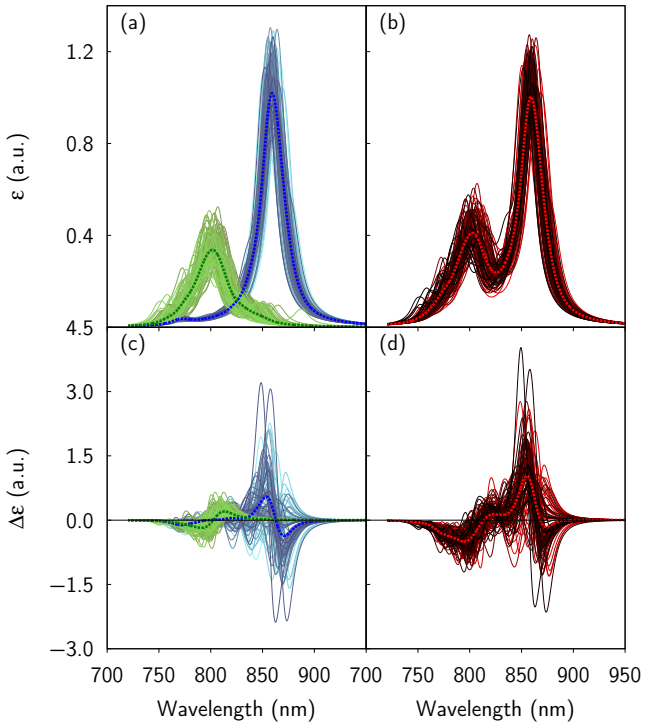

Figure 6: Average LA (a,b) and CD (c,d) spectra, plotted along with the istantaneous components. (a) and (c) show separate B800 and B850 components, whereas (b) and (d) show the coupled spectra. The spectra have been obtained as described in section 2.4 and they have been shifted in energy to match the experimental peak at $\sim$ 800 nm (energy shift = -0.05 eV).

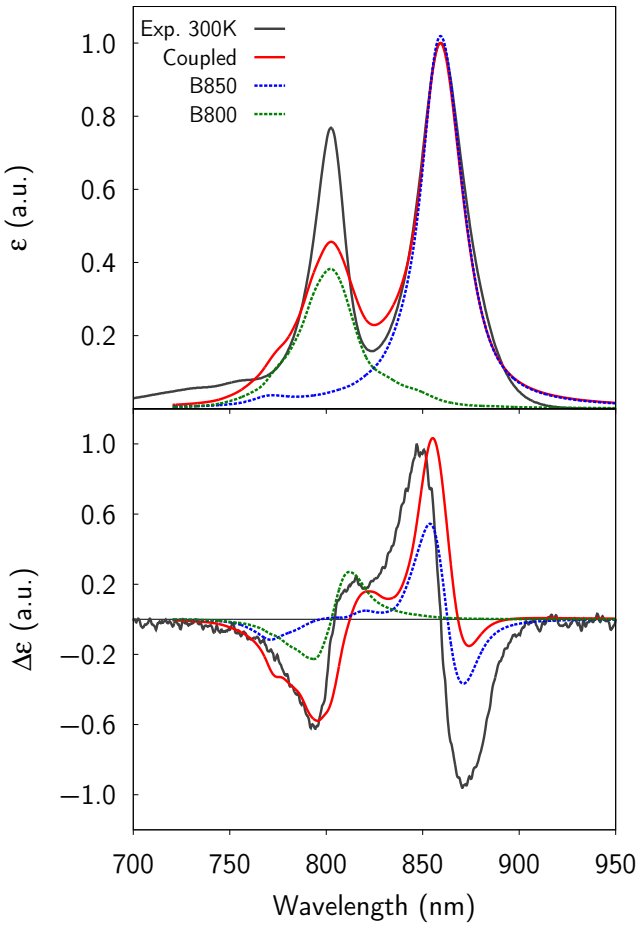

Figure 7: Excitonic LA (top) and CD (bottom) spectra of LH2 derived on the MD. The absorbance and CD intensity are given in arbitrary units and normalized to the most intense positive peak. The dashed lines represent the spectra obtained for the B800 (green) and B850 (blue) rings independently. The spectra have been shifted in energy to match the experimental peak at $\sim$ 800 nm (energy shift = -0.05 eV). The room temperature absorption and CD spectra were recorded as described in Ref.[36] using LH2 complexes from *Rps. acidophila* isolated and purified as previously described.[37]

The modeled absorption spectrum exactly matches the measured band positions. Also the width of the B850 peak matches the experiment while the B800 width is too large and the resulting ratio between the two band intensities is not correct. To test if this result could depend on the homogeneous width used, we have simulated the same spectra with very small homogeneous width, but the B800 peak remains larger than the measured one (See Figure S11 in the Supporting Information), and also larger than the B850 peak. The source of this difference is the larger inhomogeneous broadening calculated for B800 with respect to B850. Notably, we used the calculated σ_{env} values as if they were all static disorder, while they contain also a dynamic component. Unfortunately, it is not possible to univocally dissect the two contributions, if not fitting them to the experimental spectra.

The experimental CD spectrum at room temperature appears different than the low-temperature one in both broadening and relative intensities of the bands. In particular, the B800 positive band almost vanishes. Our modeled CD reproduces the overall shape of the spectrum, except the negative B850 peak, as already noted for the crystal. As already

observed for the crystal structure, the LA spectrum is almost equal to the sum of the B800 and B850 components, whereas the CD spectrum is sensitive to the inter-ring coupling, and the B850 coupled borrows rotatory strength from the B800 band. The small B800–B850 mixing happens despite the site energy differences and the static disorder, and breaks the symmetry of the B800 and B850 couplets. The only way to reproduce the asymmetrical B800 couplet is to consider some B800–B850 mixing. Unlike the spectrum obtained from the crystal structure, here the B800 couplet amplitude is nearly half of the B850 couplet. This is an effect of the energy disorder, combined with the small intra–B800 coupling.

3.3 Discussion and Conclusions

The analyses reported in the previous subsections clearly show that the two investigated models, namely that based on the crystal structure (CRY) and that using configurations generated from the MD, give quite different results.

First of all, the excitonic parameters averaged on the MD simulation are significantly different from those calculated on the crystal structure. The B850 exciton splitting reduces from 1517 to 1275 cm^{-1} (-16%) moving from the crystal to the MD description, in agreement with experimental variation between low and room temperature Davydov splittings (-13%).[2] This behavior is reflected on the absorption spectrum, where the B850 band blue shifts when the temperature is increased, whereas the B800 peak does not shift.[4] Our results show that the B850 blue shift is mainly due to a reduction of the inter-pigment couplings; in addition, the site energy difference between B800 and B850 pigments is reduced on average by $\sim$50 cm^{-1} in the MD.

The CRY and the MD-based calculations also give different descriptions of the environment effects on the excitonic parameters. In the crystal structure the environment causes a redshift of the Q_y bands of $\sim$880 cm^{-1}, with small differences among the different pigment types ($<$ 25 cm^{-1}). A redshift is also obtained along the MD, but in that case the solvatochromic shift for the B850 (α and β) is around 830 cm^{-1}, whereas the shift for B800 is 610 cm^{-1}. It has been suggested that hydrogen-bonds of the side-chains to the BChls can play an important role in differentiating them.[17] To quantify such an effect, we have repeated the calculations on three representative BChls (one from the B800 ring, and a dimer from the B850) by setting to zero both the charge and the polarizabilities of protein residues interacting through H-bond with the OBB oxygen of their acetyl group (see Figure 8). From the comparison with the full calculations, we can observe that for the B850 dimer the presence of Trp and Tyr accounts for $\sim$ 15% to the total solvatochromic shift. On the contrary, in the case of B800 pigment, the charged Arg residue contributes to $\sim$ 70% of the total shift.

Moving to the transition dipole moments, an interesting environment effect can be observed regarding their orientation. The environment does not affect the θ angle, which describes the out-of-plane tilt, but it has a non-negligible influence on the φ angle, which represents the in-plane tilt. For both the CRY and the MD descriptions, the presence of the environment induces a clockwise rotation of the transition dipole moment of -1.7° and -1.0° respectively. This means that the environment enhances the tilting of the electric dipole moment out of the NB–ND axis. However, since the changes of φ are almost the same for B850α and β, the net effect on the CD spectrum is negligible.

Another noteworthy difference found between the CRY and the MD-based descriptions is the exciton delocalization. There are various measures of exciton delocalization; one of the simplest is through the inverse participation ratio (IPR):

$$L_K = \left[\sum_{i=1}^{N} \left(C_i^K \right)^4 \right]^{-1} \qquad (8)$$

where L_K ranges from 1, for a fully localized state, to N, for a completely delocalized state. In the absence of disorder, as in the crystal structure, the delocalization lengths are close to the maximum values of 18(9) for the states $k = 0, 9$ of the B850(B800) ring, and 12(6) for the doubly degenerate states; even in the

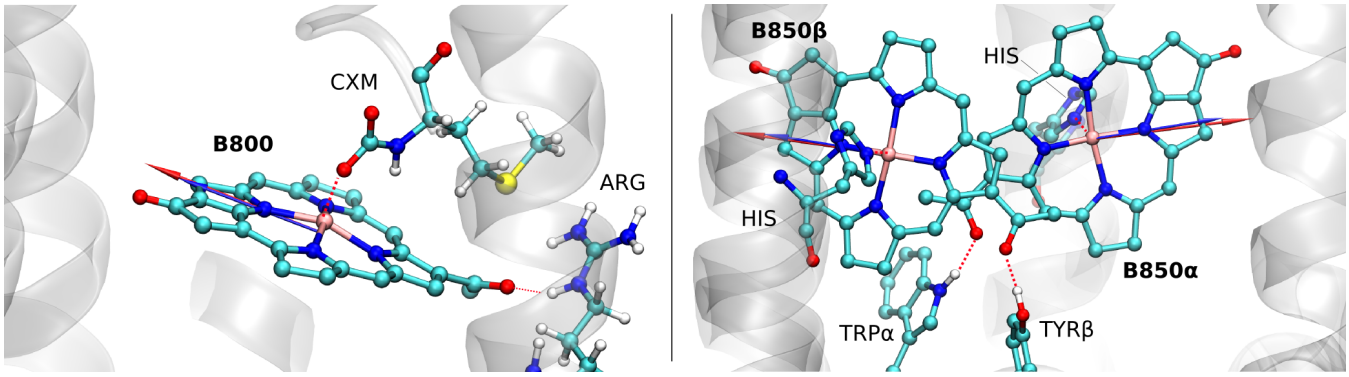

Figure 8: Schematic view of the local protein environment for the three selected BChls inside the LH2 complex. The interacting protein residues are also shown. Colored arrows refer to the direction of the electric transition dipole moments computed in vacuum (blue) and in MMPol (red) on the crystal structure.

B800 ring, despite the low couplings, the delocalization lengths are close to the maximum. Instead, adding site disorder through the MD-based model results in a localization of the exciton with a reduction of L_K. In the B850 ring, the large couplings allow the exciton to remain delocalized even in the presence of disorder: from our MD results, $L_K = 8\pm2$ sites (See Figure S10 in the Supporting Information). On the contrary, in the B800 ring the average delocalization length is ~ 1.4 sites. Our L_K is considerably lower than the values found in single-molecule spectroscopic investigations,[38] which are however measured at low temperature.

On the basis of all these findings, it is reasonable to conclude that the crystal structure and the MD simulation describe LH2 in different situations, namely, a zero-temperature limit and a room temperature average. The main features of both the absorption and CD spectra and their temperature dependence are in fact well reproduced. As it regards the CD spectra, a large sensitivity to even tiny changes in the relative orientation of the transition dipoles of the interacting BChls is found. This sensitivity unequivocally indicates that the accurate simulation of the measured CD spectrum is a real challenge for an *ab initio* approach.

Finally, our results indicate that the difference in the exciton structure of LH2 at low and high temperatures are mainly related to fluctuations in the relative orientations of the BChls (and of their interactions), rather than changes in the ring size as it was previously suggested.[2]

We can thus conclude saying that the strategy here proposed, which compares a "static" description using a single crystal structure with the one including structural and electronic fluctuations of the pigments coupled to electrostatic and polarization fluctuations of the environment, seems to be effective. It allows indeed a detailed, molecular-level, investigation of the many aspects which contribute to determine the complex excitonic character of the system and directly relates them to the shape of absorption and CD spectra and their temperature-dependent changes.

Supporting Information

Details on the MD simulation; Tables S1–S2 show other results about the CT analysis performed on crystal structure; Exciton structure of LH2 is reported in Table S3; Table S4 compares the electronic couplings obtained in this work with previous data sets; Figure S1–S5 show the analysis of MD trajectory; Figure S6 compares exciton CD spectra obtained with different level of theories; Figure S7–S10 show the results of DOS analysis; Figure S11 compares the absorption spectra obtained with different HWHM Lorentzian profiles.

Acknowledgments

L.C, S.J, C.G., S.C., M.C and B.M. kindly acknowledge the European Research Council (ERC) for financial support in the framework of the Starting Grant (EnLight–277755). RJC and ATG gratefully acknowledge funding from the Photosynthetic Antenna Research Center (PARC), an Energy Frontier Research Center funded by the Department of Energy, Office of Science, Office of Basic Energy Sciences under award number DE-SC0001035.

References

(1) Georgakopoulou, S.; Frese, R. N.; Johnson, E.; Koolhaas, C.; Cogdell, R. J.; van Grondelle, R.; van der Zwan, G. Absorption and CD Spectroscopy and Modeling of Various LH2 Complexes from Purple Bacteria. *Biophys. J.* **2002**, *82*, 2184–2197.

(2) Pajusalu, M.; Rätsep, M.; Trinkunas, G.; Freiberg, A. Davydov Splitting of Excitons in Cyclic Bacteriochlorophyll a Nanoaggregates of Bacterial Light-Harvesting Complexes between 4.5 and 263 K. *ChemPhysChem* **2011**, *12*, 634–644.

(3) Kunz, R.; Timpmann, K.; Southall, J.; Cogdell, R. J.; Köhler, J.; Freiberg, A. Fluorescence-Excitation and Emission Spectra from LH2 Antenna Complexes of *Rhodopseudomonas acidophila* as a Function of the Sample Preparation Conditions. *J. Phys. Chem. B* **2013**, *117*, 12020–12029.

(4) Trinkunas, G.; Zerlauskiene, O.; Urbonienė, V.; Chmeliov, J.; Gall, A.; Robert, B.; Valkunas, L. Exciton Band Structure in Bacterial Peripheral Light-Harvesting Complexes. *J. Phys. Chem. B* **2012**, *116*, 5192–5198.

(5) Curutchet, C.; Mennucci, B. Quantum Chemical Studies of Light Harvesting. *Chem. Rev.* **2016**, DOI: 10.1021/acs.chemrev.5b00700.

(6) Curutchet, C.; Scholes, G. D.; Mennucci, B.; Cammi, R. How solvent controls electronic energy transfer and light harvesting: toward a quantum-mechanical description of reaction field and screening effects. *J. Phys. Chem. B* **2007**, *111*, 13253–13265.

(7) Krueger, B. P.; Scholes, G. D.; Fleming, G. R. Calculation of Couplings and Energy-Transfer Pathways between the Pigments of LH2 by the ab Initio Transition Density Cube Method. *J. Phys. Chem. B* **1998**, *102*, 5378–5386.

(8) Scholes, G. D.; Gould, I. R.; Cogdell, R. J.; Fleming, G. R. Ab initio molecular orbital calculations of electronic couplings in the LH2 bacterial light-harvesting complex of *Rps. acidophila*. *J. Phys. Chem. B* **1999**, *103*, 2543–2553.

(9) Tretiak, S.; Middleton, C.; Chernyak, V.; Mukamel, S. Exciton Hamiltonian for the Bacteriochlorophyll System in the LH2 Antenna Complex of Purple Bacteria. *J. Phys. Chem. B* **2000**, *104*, 4519–4528.

(10) Tretiak, S.; Middleton, C.; Chernyak, V.; Mukamel, S. Bacteriochlorophyll and Carotenoid Excitonic Couplings in the LH2 System of Purple Bacteria. *J. Phys. Chem. B* **2000**, *104*, 9540–9553.

(11) Neugebauer, J. Photophysical Properties of Natural Light-Harvesting Complexes Studied by Subsystem Density Functional Theory. *J. Phys. Chem. B* **2008**, *112*, 2207–2217.

(12) Olbrich, C.; Kleinekathöfer, U. Time-dependent atomistic view on the electronic relaxation in light-harvesting system II. *J. Phys. Chem. B* **2010**, *114*, 12427–12437.

(13) van der Vegte, C. P.; Prajapati, J. D.; Kleinekathöfer, U.; Knoester, J.; Jansen, T. L. C. Atomistic modeling of two-dimensional electronic spectra and excited-state dynamics for a light harvesting 2 complex. *J. Phys. Chem. B* **2015**, *119*, 1302–1313.

(14) Jurinovich, S.; Curutchet, C.; Mennucci, B. The Fenna-Matthews-Olson Protein Revisited: A Fully Polarizable (TD)DFT/MM Description. *ChemPhysChem* **2014**, *15*, 3194–3204.

(15) Jurinovich, S.; Viani, L.; Curutchet, C.; Mennucci, B. Limits and potentials of quantum chemical methods in modelling photosynthetic antennae. *Phys. Chem. Chem. Phys.* **2015**, *17*, 30783–30792.

(16) Jurinovich, S.; Viani, L.; Guarnetti-Prandi, I.; Renger, T.; Mennucci, B. Towards an ab initio description of the optical spectra of light-harvesting antennae: application to the CP29 complex of photosystem II. *Phys. Chem. Chem. Phys.* **2015**, *17*, 14405–14416.

(17) Cogdell, R. J.; Gall, A.; Köhler, J. The architecture and function of the light-harvesting apparatus of purple bacteria: from single molecules to in vivo membranes. *Q. Rev. Biophys.* **2006**, *39*, 227–324.

(18) Papiz, M. Z.; Prince, S. M.; Howard, T.; Cogdell, R. J.; Isaacs, N. W. The Structure and Thermal Motion of the B800–850 LH2 Complex from *Rps. acidophila* at 2.0Å Resolution and 100K: New Structural Features and Functionally Relevant Motions. *J. Mol. Biol.* **2003**, *326*, 1523–1538.

(19) Case, D. et al. *Amber14*; University of California, San Francisco., CA, 2015.

(20) Ogata, K.; Yuki, T.; Hatakeyama, M.; Uchida, W.; Nakamura, S. All-atom molecular dynamics simulation of photosystem II embedded in thylakoid membrane. *J. Am. Chem. Soc.* **2013**, *135*, 15670–15673.

(21) Dickson, C. J.; Madej, B. D.; Skjevik, A. a.; Betz, R. M.; Teigen, K.; Gould, I. R.; Walker, R. C. Lipid14: The Amber Lipid Force Field. *J. Chem. Theory Comput.* **2014**, *10*, 865–879.

(22) Hornak, V.; Abel, R.; Okur, A.; Strockbine, B.; Roitberg, A.; Simmerling, C. Comparison of multiple Amber force fields and development of improved protein backbone parameters. *Proteins: Struct., Funct., Bioinformatics* **2006**, *65*, 712–725.

(23) Ceccarelli, M.; Procacci, P.; Marchi, M. An ab initio force field for the cofactors of bacterial photosynthesis. *J. Comput. Chem.* **2003**, *24*, 129–142.

(24) Guarnetti-Prandi, I.; Viani, L.; Andreussi, O.; Mennucci, B. Combining classical MD and QM methods for the description of electronic excitations: the case of carotenoids. *J. Comput. Chem.* **2015**, *37*, 981–991.

(25) Humphrey, W.; Dalke, A.; Schulten, K. VMD – Visual Molecular Dynamics. *J. Mol. Graphics* **1996**, *14*, 33–38.

(26) Frisch, M. J. et al. *Gaussian 09*, Revision D.01; Gaussian, Inc: Wallingford, CT, 2009.

(27) Iozzi, M. F.; Mennucci, B.; Tomasi, J.; Cammi, R. Excitation energy transfer (EET) between molecules in condensed matter: a novel application of the polarizable continuum model (PCM). *J. Chem. Phys.* **2004**, *120*, 7029–7040.

(28) Curutchet, C.; Muñoz Losa, A.; Monti, S.; Kongsted, J.; Scholes, G. D.; Mennucci, B. Electronic Energy Transfer in Condensed Phase Studied by a Polarizable QM/MM Model. *J. Chem. Theory Comput.* **2009**, *5*, 1838–1848.

(29) List, N. H.; Curutchet, C.; Knecht, S.; Mennucci, B.; Kongsted, J. Toward Reliable Prediction of the Energy Ladder in Multichromophoric Systems: A Benchmark Study on the FMO Light-Harvesting Complex. *J. Chem. Theory Comput.* **2013**, *9*, 4928–4938.

(30) Jurinovich, S.; Cupellini, L.; Guido, C. A.; Mennucci, B. *EXAT*

- *EXcitonic Analysis Tool*, 2016. http://www1.dcci.unipi.it/molecolab/tools/.

(31) Jurinovich, S.; Guido, C. A.; Bruhn, T.; Pescitelli, G.; Mennucci, B. The role of magnetic-electric coupling in exciton-coupled ECD spectra: the case of bisphenanthrenes. *Chem. Commun.* **2015**, *51*, 10498–10501.

(32) Yang, C.-H.; Hsu, C.-P. A multi-state fragment charge difference approach for diabatic states in electron transfer: extension and automation. *J. Chem. Phys.* **2013**, *139*, 154104.

(33) Kenny, E. P.; Kassal, I. Benchmarking Calculations of Excitonic Couplings between Bacteriochlorophylls. *J. Phys. Chem. B* **2016**, *120*, 25–32.

(34) Anda, A.; Hansen, T.; De Vico, L. Multireference Excitation Energies for Bacteriochlorophylls A within Light Harvesting System 2. *J. Chem. Theory Comput.* **2016**, *12*, 1305–1313.

(35) Bopp, M. A.; Sytnik, A.; Howard, T. D.; Cogdell, R. J.; Hochstrasser, R. M. The dynamics of structural deformations of immobilized single light-harvesting complexes. *Proc. Natl. Acad. Sci. U. S. A.* **1999**, *96*, 11271–11276.

(36) Cogdell, R. J.; Hawthornthwaite, A. M.; Evans, M. B.; Ferguson, L. A.; Kerfeld, C.; Thornber, J.; van Mourik, F.; van Grondelle, R. Isolation and characterisation of an unusual antenna complex from the marine purple sulphur photosynthetic bacterium Chromatium purpuratum BN5500. *Biochim. Biophys. Acta, Bioenerg.* **1990**, *1019*, 239–244.

(37) Cogdell, R. J.; Durant, I.; Valentine, J.; Lindsay, J.; Schmidt, K. The isolation and partial characterisation of the light-harvesting pigment-protein complement of *Rhodopseudomonas acidophila*. *Biochim. Biophys. Acta, Bioenerg.* **1983**, *722*, 427–435.

(38) van Oijen, A.; Ketelaars, M.; Köhler, J.; Aartsma, T.; Schmidt, J. Spectroscopy of individual LH2 complexes of *Rhodopseudomonas acidophila*: localized excitations in the B800 band. *Chem. Phys.* **1999**, *247*, 53–60.

Graphical TOC Entry